Theory of line shapes of exciton resonances in semiconductor superlattices

Hanyou Chu and Yia-Chung Chang
Department of Physics and Materials Research Laboratories, University of Illinois at Urbana-Champaign, Urbana, Illinois 61801
(Received 8 December 1988)

Realistic model calculations on the absorption spectra of semiconductor superlattices are presented. Emphasis is put on the analysis of line shapes of various peak structures arising from discrete excitonic states of one pair of subbands coupled with the excitonic (discrete and continuum) states associated with other pairs of subbands. The angle-dependent valence-band mixing and the final-state interaction effects are properly taken into account via the **k**-space sampling technique. Our results are in excellent agreement with recent high-resolution photoluminescence excitation spectra for a number of GaAs-$Al_xGa_{1-x}As$ quantum wells and superlattices.

I. INTRODUCTION

Optical measurements including photoabsorption, photoluminescence, and Raman scattering have been widely used for probing the electronic states of superlattices and quantum wells. The general features in the absorption spectra for a quantum well can be easily interpreted by using a simple effective-mass (particle-in-a-box) model,[1] which assumes parabolic band structures for both the electrons and holes. In this model, the oscillator strengths for the band-to-band transitions are proportional to

$$F_{nn'} \equiv \langle f_n | g_{n'} \rangle \approx F_n \delta_{nn'} , \tag{1}$$

where f_n and g_n are the envelope functions of the nth electron and hole subbands, respectively. Thus the interband transitions are allowed only when the conduction- and valence-subband states have the same principal quantum number. Associated with each pair of conduction and valence subbands there exists an exciton state which appears in the absorption spectrum as a prominent peak. Ignoring the coupling between excitonic states derived from different pairs of conduction and valence subbands, one expects the $\Delta n = 0$ selection rule to hold for the excitonic transitions as well. Indeed, most experimental data indicate that $\Delta n = 0$ excitonic transitions are at least an order of magnitude stronger than the other excitonic transitions which violate this selection rule.

Recent studies[2,3] of the electronic and optical properties of semiconducting quantum wells have revealed that the mixing of heavy- and light-hole components (valence-band mixing) in the quantum well (or superlattice) states can lead to $\Delta n \neq 0$ (forbidden) interband transitions with strengths much larger than those expected from the simple particle-in-the-box model. The most pronounced $\Delta n \neq 0$ transition is associated with the excitonic states involving the second conduction subband (CB2) and the first light-hole (LH1) subband which mix strongly with the second heavy-hole (HH2) subband. Here the labels LH1 and HH2 are used based on the symmetry properties of the subbands at $\mathbf{k}_{\parallel} = \mathbf{0}$. When $\mathbf{k}_{\parallel} \neq \mathbf{0}$ the superlattice valence-band states in general contain admixtures of heavy- and light-hole characters. Ignoring the coupling of excitons derived from different pairs of subbands but keeping the mixing of heavy- and light-hole states, Sanders and Chang[3] calculated the absorption spectra of GaAs-$Al_xGa_{1-x}As$ quantum wells. The results indicate that the excitons associated with the second conduction subbands will contain a doublet structure, one derived from the HH2 states and the other derived from the LH1 states. As a result of strong valence-band mixing, the two peak structures have comparable oscillator strengths for well width around 111 Å. The theoretical predictions are in reasonable agreement with the high-resolution photoluminescence excitation spectra.[4]

The theory of Sanders and Chang, however, omitted the angular dependence of the mixing coefficient in the coupled-valence-subband states. Although this does not affect the valence-subband structures very much, it changes the selection rules for the exciton angular momentum. A theory which incorporates the angular dependence into the excitonic states was recently developed by Zhu and Huang,[5] and the oscillator strengths of excitonic transitions were analyzed by Zhu.[6] It was shown that as a result of the angle-dependent valence-band mixing, the p-like light-hole states are coupled to the s-like heavy-hole states.[6] Thus, the $2p$ LH1-CB2 exciton is allowed (via the mixing with the $1s$ HH2-CB2 exciton), whereas the $1s$ LH1-CB2 exciton is forbidden. However, the oscillator strength for the $2p$ LH1-CB2 exciton calculated in Zhu's theory is too small to account for the prominent doublet structure observed by Miller *et al.*[4] As we shall show in this paper, the line shapes and oscillator strengths for the HH2-CB2 exciton doublet can be reproduced theoretically by taking into account the angle-dependent valence-band mixing and the coupling of excitonic states (discrete plus continuum) associated with different pairs of subbands.

There are added complications for the excitonic effect in semiconductor superlattices where electronic states derived from different quantum wells are coupled to form a series of minibands instead of discrete energy levels. At the minizone boundaries, the lowest subband energy is a maximum along the growth (z) direction, but a minimum along the in-plane (x or y) direction. Thus, we

have M_1 saddle points there. In the past, excitonic effects associated with the M_1 saddle point in bulk semiconductors have attracted a great deal of interest both theoretically and experimentally.[7-12] It is found that the resonant photoabsorption peaks can be formed below the saddle point which is called saddle-point excitons.[7] Theoretical studies of this phenomenon via a contact-potential model[8] and adiabatic model[10] have been reported. Recently, we have developed a **k**-space sampling method which allows quantitative calculations of the absorption spectra associated with the saddle-point states in solids including the realistic Coulomb interaction.[13] In this paper we further extend this method to calculate the absorption spectra for a superlattice system, including the valence-band mixing and the coupling of exciton states associated with different pairs of subbands.

II. k-SPACE SAMPLING METHOD FOR EXCITONS IN SUPERLATTICES

We shall first consider the excitonic states derived from a pair of conduction and valence subbands of a superlattice. Since the photons absorbed have a negligible momentum, only excitonic states with zero total momentum are needed in the calculation of absorption coefficient. In general, the zero-momentum excitonic states can be written as linear combinations of electron-hole product states associated with electron wave vector **k** and hole wave vector $-\mathbf{k}$. In the **k**-space sampling method, we divide the entire Brillouin zone into a large number of small segments of the same volume. We define a basis state β_j to be the average of all the electron-hole product states with wave vector **k** located inside segment j, viz.,

$$\beta_j=\sum_{\mathbf{k}\in\Delta_j}|\mathbf{k}\rangle/\sqrt{\Omega}\ , \tag{2}$$

where $\mathbf{k}\in\Delta_j$ means that **k** belongs to segment j, and $\Omega\equiv\sum_{\mathbf{k}\in\Delta_j}$. We then expand the exciton state Ψ in the set of basis state $\{\beta_j\}$, i.e., $\Psi=\sum_j G(\mathbf{k}_j)\beta_j$. Substituting this expansion into the Schrödinger equation for Ψ immediately leads to an eigenvalue problem:

$$\sum_{j'}\overline{H}_{j,j'}G(\mathbf{k}_{j'})=EG(\mathbf{k}_j)\ , \tag{3}$$

with

$$\overline{H}_{j,j'}=\frac{\sum_{\mathbf{k}\in\Delta_j}\sum_{\mathbf{k}\in\Delta_j}\langle\mathbf{k}|H|\mathbf{k}'\rangle}{\Omega}\ , \tag{4}$$

where $\langle\mathbf{k}|H|\mathbf{k}'\rangle$ is the exciton Hamiltonian matrix element between the electron-hole product states $|\mathbf{k}\rangle$ and $|\mathbf{k}'\rangle$. Solving the above eigenvalue problem yields the energies and corresponding wave functions for a few low-lying discrete exciton states and a good sampling of the continuum states. The absorption coefficient for interband transitions can be written as:

$$\alpha(\hbar\omega)=\frac{C}{\omega}\sum_i|\langle\Psi_i|\hat{\epsilon}\cdot\mathbf{p}|G\rangle|^2\,\delta(E_i-\hbar\omega)\ , \tag{5}$$

where C is a constant, $\hat{\epsilon}$ is the polarization vector, G denotes the ground state of the solid, and Ψ_i denotes the ith excitonic states with energy eigenvalue E_i. Here the label i runs through discrete states as well as continuum states. Assuming the momentum matrix elements between the conduction- and valence-band Bloch states to be independent of **k**, we obtain

$$\langle\Psi_i|\hat{\epsilon}\cdot\mathbf{p}|G\rangle=P_{cv}(\hat{\epsilon})\sum_{\mathbf{k}}G(\mathbf{k})\ ,$$

where $P_{cv}(\hat{\epsilon})$ is the valence-to-conduction-band momentum matrix element for photons with polarization $\hat{\epsilon}$.

To minimize the size of the matrix to be diagonalized, while maintaining the high precision, the symmetry of the system is fully exploited. Note that the absorption spectrum only depends on $\sum_{\mathbf{k}}G(\mathbf{k})$, which is nonzero only for states with full symmetry of the system. Within the approximations used, the superlattice has a circular symmetry in parallel directions and a reflection symmetry in the growth direction. We then use symmetrized basis states labeled by the radial component of $\mathbf{k}_\parallel$ and the growth direction component q. A cutoff Λ is introduced for the sampling of $k_\parallel$. The final results for energies near the saddle point are insensitive to the choice of the cutoff, as long as Λ is large enough.

In order to obtain a smooth absorption spectrum, we replace the δ function in Eq. (5) by a Lorentzian function with a half-width Γ, viz.,

$$\delta(E_i-E)\approx\Gamma/\{\pi[(E_i-E)^2+\Gamma^2]\}\ . \tag{6}$$

The magnitude of Γ is roughly equal to the energy spacing of the eigenstates. The calculated results for a series of ideal superlattices (with spherical subbands) are reported in our previous paper.[13] For realistic superlattices, we must consider the mixing and anisotropy of valence subbands which is the subject of the next section.

III. EXCITON HAMILTONIAN AND RECURSION METHOD

In this section we describe the details of the exciton Hamiltonian, and we consider the coupling of excitonic states associated with different pairs of subbands. For superlattices of interest here, such coupling is appreciable only for excitonic states associated with different valence subbands, but the same conduction subband. This is because the energy separation between consecutive conduction subbands is much larger than the exciton binding energy.

We denote the superlattice wave vector by **k**, its projection in the growth direction by q, and its in-plane projection by $\mathbf{k}_\parallel$. In the envelope-function approximation, we write the nth conduction subband state at wave vector $\mathbf{k}=(\mathbf{k}_\parallel,q)$ as

$$\Psi^e_{n,\mathbf{k}}=\sum_{k_z}e^{i\mathbf{k}\cdot\rho+ik_zz}f_{n,q}(k_z)|u_C\rangle\ ,$$

where $|u_C\rangle$ denotes the zone-center Bloch state of the well material. Note that due to the supperlattice periodicity in the z direction, k_z in the above summations must be equal to a superlattice reciprocal lattice vector, i.e.,

$$k_z = s(\pi/d), \quad s = \text{integer} ,$$

where d is the length of the superlattice unit cell. The Fourier transform of $f_{n,q}(k_z)$ satisfies the simple effective-mass equation:

$$\left[\frac{\hbar^2}{2m_e(z)}(k_\parallel^2 - \partial^2/\partial z^2) + V_e(z)\right] f_{n,q}(z) = E_n^e(\mathbf{k}_\parallel, q) f_{n,q}(z) , \quad (7)$$

where $V_e(z_e)$ is the superlattice potential for the electron and $m_e(z)$ is the effective electron mass in GaAs or $Al_xGa_{1-x}As$ depending on where z is located. Note that in this approximation, the envelope function f_n is independent of $\mathbf{k}_\parallel$.

The mth valence-subband state at wave vector $\mathbf{k}$ (or hole state at $-\mathbf{k}$) can be written as

$$\Psi^h_{m,-\mathbf{k}} = \sum_{\nu,k_z} e^{i\mathbf{k}_\parallel\cdot\rho + ik_z z} g^\nu_{m,\mathbf{k}_\parallel}(k_z)|u_\nu\rangle , \quad (8)$$

where $\{|u_\nu\rangle; \nu = \frac{3}{2}, \frac{1}{2}, -\frac{1}{2}, -\frac{3}{2}\}$ are four bulk Bloch states at the valence-band maximum for the well material. The envelope function $g^\nu_{m,\mathbf{k}}(k_z)$ satisfies a multiband effective mass equation in $\mathbf{k}$ space, viz.,

$$\sum_{\nu'}[-H^{(V)}_{\nu,\nu'}(\mathbf{k}_\parallel, k_z) - E^h_m(\mathbf{k}_\parallel)\delta_{\nu,\nu'}] g^{\nu'}_{m,\mathbf{k}}(k_z) + \sum_{k_z'} \langle k_z|V_h(z)|k_z'\rangle g^\nu_{m,\mathbf{k}}(k_z') = 0 , \quad (9)$$

where $V_h(z)$ is the superlattive potential seen by the hole and $H^{(V)}_{\nu,\nu'}(\mathbf{k}_\parallel, k_z)$ are matrix elements of the Luttinger-Kohn Hamiltonian[14] for describing the bulk valence-band structure.

Note that at $\mathbf{k}_\parallel = 0$, the off-diagonal elements of the Luttinger-Kohn Hamiltonian vanish, and the four components $\nu = \frac{3}{2}, \frac{1}{2}, -\frac{1}{2}, -\frac{3}{2}$ are decoupled. We define the mth eigenstate associated with the νth diagonal component of the hole Hamiltonian (the zeroth-order hole Hamiltonian) at $\mathbf{k}$ as

$$\Psi^{h0}_{m,\nu,-\mathbf{k}} = \sum_{k_z} e^{i\mathbf{k}_\parallel\cdot\rho + ik_z z} g^\nu_{m,q}(k_z)|u_\nu\rangle .$$

The corresponding energy eigenvalues are denoted by $-E^0_{m,\nu}(\mathbf{k})$. In analogy to the $\mathbf{k}\cdot\mathbf{p}$ theory, one can solve the superlatttice valence-subband states approximately by expanding them in terms of the zeroth-order solutions. In the zeroth-order approximatiom, we have well-defined heavy-hole (HH) and light-hole (LH) subbands, and they are labeled according to their characters and principal quantum numbers. For example, HHn and LHn denote the nth heavy- and light-hole subbands, respectively. Similarly, the nth conduction subband will be denoted CBn. At $\mathbf{k}_\parallel \neq 0$, the off-diagonal elements of the Kohn-Luttinger Hamiltonian mix the zeroth-order solutions; thus each valence subband contains admixtures of heavy- and light-hole characters. Examining the Kohn-Luttinger Hamiltonian, one finds that the coupling term is angle dependent.

To make the computation more feasible, we adopt the axial approximation introduced by Altarelli.[15] With this approximation the valence-subband structure has circular symmetry in the x-y plane. It can be shown that within the axial model the angle-dependent coupling can be incorporated by explicitly introducing an angle-dependent phase factor in the envelope functions, viz.,

$$g^\nu_{m,\mathbf{k}_\parallel}(k_z) = \bar{g}^\nu_{m,k_\parallel}(k_z) e^{i(1/2-\nu)\phi} ,$$

where $\nu = \frac{3}{2}, \frac{1}{2}, -\frac{1}{2}, -\frac{3}{2}$, and ϕ is the angle between $\mathbf{k}_\parallel$ and the x axis (the azimuthal angle for $\mathbf{k}$). Thus in an exciton state, different components of the valence-band envelope function must be associated with different angular momenta. For example, an s-like $\nu = \frac{3}{2}$ (heavy-hole-like) envelope function must be coupled to a p-like $\nu = \frac{1}{2}$ (light-hole-like) envelope function. As a consequence, the parity-forbidden LH1-CB2 excitonic transition must have an orbital angular momentum $l = 1$, as it is coupled to the s-like HH2-CB2 excitonic transition.

Since different valence subbands are also coupled by the electron-hole Coulomb interaction, we lose no generality by expanding the excitonic states in terms of electron-hole product states containing eigenstates of the zeroth-order hole Hamiltonian. Thus, the excitonic states associated with conduction subband n is written as

$$\Psi^n = \sum_{m,\nu}\sum_{\mathbf{k}} G^n_{m,\nu}(\mathbf{k}) \Psi^e_{n,\mathbf{k}} \Psi^{h0}_{m,\nu,-\mathbf{k}} , \quad (10)$$

where ϕ is the azimuthal angle of $\mathbf{k}$. It can be shown that the expansion coefficients $G^n_{m,\nu}(\mathbf{k})$ satisfy the following effective-mass equation:

$$[E^e_n(\mathbf{k}) - E^0_{m,\nu}(\mathbf{k}) - E^{ex}_n] G^n_{m,\nu}(\mathbf{k}) + \sum_{m',\nu',\mathbf{k}'} \left[v^n_{m,m',\nu}(\mathbf{k};\mathbf{k}')\delta_{\nu,\nu'} - \sum_{k_z} H^{(\text{off})}_{\nu,\nu'}(\mathbf{k}_\parallel, k_z) g^\nu_{m,q}(k_z) g^{\nu'}_{m',q}(k_z)\delta_{\mathbf{k},\mathbf{k}'} \right] G^n_{m',\nu'}(\mathbf{k}') = 0 , \quad (11)$$

where $H^{(\text{off})}_{\nu,\nu'}(\mathbf{k}_\parallel, k_z)$ are off-diagonal matrix elements of the Kohn-Luttinger Hamiltonian. v denotes the electron-hole Coulomb interaction whose matrix elements are given by

$$v^n_{m,m',\nu}(\mathbf{k};\mathbf{k}') = -\frac{4\pi e^2}{\epsilon}\sum_s F^e_n(q, q' - sK) F^h_{\nu,m,m'}(q, q' - sK) \frac{1}{|\mathbf{k}_\parallel - \mathbf{k}'_\parallel|^2 + (q - q' + sK)^2} , \quad (12)$$

where

$$F^e_n(q,q') = \int_P dz\, f_q(z) f^*_{q'}(z) e^{-i(q-q')z} , \quad (13)$$

and

$$F^{h}_{\nu,m,m'}(q,q')=\int_P dz\, g^{\nu}_{m,q}(z)g^{\nu*}_{m',q'}(z)e^{-i(q-q')z}\ . \tag{14}$$

Here $K=\pi/d$, and s runs through all integers. The symbol $\int_P$ indicates that the integral over z is restricted in one period of the superlattice. The integrals in Eqs. (13) and (14) can be carried out analytically. For reasons given above, the coupling between excitonic states associated with different conduction subbands has been ignored. We have assumed that the dielectric constants in the well and barrier materials are the same. This a good approximation, since we are only interested in GaAs-$Ga_{1-x}Al_xAs$ superlattice with small Al mole fraction. The series in Eq. (12) converges fast since the terms involved in this series are proportional to $1/s^6$ when s is large. For higher subbands and large period superlattices, to ensure a good convergence it might be desirable to write the above formula in a different form

$$v^{n}_{m,m',\nu}(\mathbf{k},\mathbf{k}')=-\frac{4\pi e^2}{\epsilon}\int_P dz_e\int_P dz_h\, f_{n,q}(z_e)f^{*}_{n,q'}(z_e)g^{\nu*}_{m,q}(z_h)g^{\nu}_{m',q'}(z_h)V(k_{\parallel},q-q',z_e-z_h)\ ,$$

where $f_{n,q}(z)$ and $g^{\nu}_{m,q}(z)$ are the electron and hole envelope functions, respectively,

$$V(k_{\parallel},q,z)=\frac{1}{k_{\parallel}}\left[e^{-k_{\parallel}|z|}+\frac{e^{-k_{\parallel}z}}{e^{K}-1}+\frac{e^{k_{\parallel}z}}{e^{K^*}-1}\right],$$

and $K=(k_{\parallel}-iq)d$.

The exciton expansion coefficients $G^{n}_{m,\nu}(\mathbf{k})$ can be written as the product of a radial function and an angular function which depends on the orbital angular momentum of the exciton,

$$G^{n}_{m,\nu}(\mathbf{k})=G^{n}_{m,\nu}(k_{\parallel},q)e^{i(l+\nu_0-\nu)\phi},$$

where ν_0 is the predominant hole component in the exciton state and l is the exciton orbital angular momentum for that component. For example, for the $2p$ LH1-CB1 exciton state, we have $\nu_0=\frac{1}{2}$ (or $-\frac{1}{2}$) and $l=1$ (or $l=-1$). Note that this exciton state contains admixtures of s-like heavy-hole conduction-band product states, since the phase factor equals to 1 when $\nu=\frac{3}{2}$ (or $\nu=-\frac{3}{2}$). In our $\mathbf{k}$-space sampling method we only have to sample the radial component of $\mathbf{k}_{\parallel}$ and q to determine the coefficients $G^{n}_{m,\nu}(k_{\parallel},q)$. We can further simplify the problem by exploiting the reflection symmetry in the growth direction. We define symmetric and antisymmetric electron-hole product basis states as

$$|n,l,m,\nu;\mathbf{k}_{\parallel},q\rangle_{\pm}=e^{il\phi}(\Psi^{e}_{n,\mathbf{k}_{\parallel},q}\Psi^{h0}_{m,\nu,-\mathbf{k}_{\parallel},-q}\pm\Psi^{e}_{n,\mathbf{k}_{\parallel},-q}\Psi^{h0}_{m,\nu,-\mathbf{k}_{\parallel},q'})\ . \tag{15}$$

We divide the basis states into two sets, one including symmetric product states with $\nu=\frac{3}{2},-\frac{1}{2}$ and antisymmetric product states with $\nu=\frac{1}{2},-\frac{3}{2}$, and the other including antisymmetric product states with $\nu=\frac{3}{2},-\frac{1}{2}$ and symmetric product states with $\nu=\frac{1}{2},-\frac{3}{2}$. The two sets of states are decoupled, and the energy spectra produced by using either set are the same (Kramer's degeneracy). In this scheme, the size of the Hamiltonian is reduced by a factor of 2. For quantum-well cases, the above Hamiltonian can be further simplified. For instance, the coupling between the HH1 and HH2 states due to the Coulomb interaction vanishes by symmetry.

We shall consider excitonic states with orbital angular momenta $|l|=0$ and 1 (i.e., s- and p-like) only. The higher-angular-momentum states are much less important in the calculation of the absorption coefficient.[6] Thus, the Coulomb matrix elements involving the $|l|\geq 2$ states are ignored. Due to symmetry, the two sets of excitonic states described by $\{(s\text{-like},\ |\nu|=\frac{3}{2}),\ (p\text{-like},\ |\nu|=\frac{1}{2})\}$ and $\{(p\text{-like},\ |\nu|=\frac{3}{2}),\ (s\text{-like},\ |\nu|=\frac{1}{2})\}$ are decoupled. In principle, many zeroth-order valence-subband states of different m values are needed in the expansion of the exciton states to obtain accurate results. In practice, it suffices to include only a few valence subbands for the energy range of interest. For calculating the absorption spectra we typically include both s- and p-like excitonic states associated with HH1, HH2, HH3, LH1, and LH2 valence subbands. The derivations for the matrix elements for the kinetic energy terms are straightforward, and those for the Coulomb interaction are given in the Appendix.

Since the number of basis states required to produce an accurate absorption spectrum is quite large (more than 1000), the brute-force matrix diagonalization is impractical. From Eq. (5) we see that the absorption coefficient can be written as the imaginary part of the Green's function at $\mathbf{r}=0$. Thus the recursion method[16] can be used to calculate the projected density of states. The recursion method, or alternatively the Lanczos method, is not suitable for obtaining exact energy states except for the band edges. But it gives a good description of projected density of states, and this is just what we are after. In this method we start from an initial state $|0\rangle$ on which the density of states is to be projected. The state is then to be multiplied by the Hamiltonian operator of the system, and the resulting state is orthogonalized with the previous ones. This is repeated for N steps, where N is the dimension of a finite system. If the dimension of the Hamiltonian is infinite, the iteration has to be stopped at some point and a suitable termination function should be introduced to produce the best results. The Hamiltonian is thus tridiagonalized, and the Green's function can be calculated directly by a continued fraction scheme. The algorithm is stated in the following. Let $|n\rangle$ be the basis state generated at the nth step and $|u_n\rangle\equiv H|n\rangle$. We define

$$|1\rangle=\frac{1}{b_0}(|u_0\rangle-a_0|0\rangle)$$

and

$$|n+1\rangle=\frac{1}{b_n}(|u_n\rangle-a_n|n\rangle-b_{n-1}|n-1\rangle) \quad \text{for } n>1$$

with

$$a_n=\langle n|H|n\rangle=\langle n|u_n\rangle$$

and

$$b_n=(\langle u_n|u_n\rangle-a_n^2-b_{n-1}^2)^{1/2} ,$$

where $|0\rangle$ is the initial state. The iteration should be stopped when $b_n=0$. The (tridiagonal) Hamiltonian matrix in the new set of basis states $\{|n\rangle\}$ becomes

$$H=\begin{bmatrix} a_0 & b_0 & & & & & \\ b_0 & a_1 & b_1 & & & & \\ & b_1 & a_2 & b_2 & & & \\ & & \cdots & \cdots & \cdots & & \\ & & & b_{n-1} & a_n & b_n & \\ & & & & \cdots & \cdots & \cdots \end{bmatrix} .$$

The Green's function projected in state $|0\rangle$ is then given by

$$\langle 0|G(E)|0\rangle=\cfrac{1}{E-a_0-\cfrac{b_0^2}{E-a_1-\cfrac{b_1^2}{E-a_2-\ddots\cfrac{b_{N-1}^2}{E-a_N-b_N^2 t(E)}}}} ,$$

where the function $t(E)$ represents a termination function of the continued fraction after N iterations and is zero if the system is finite. In calculating the Green's function a broadening procedure similar to that given in Eq. (6) is still needed. This can be done by replacing E with $E+i\Gamma$, where Γ is the half width for broadening. Mathematically, this algorithm is exact, but numerically it is unstable due to the round-off error so that only the smallest and the largest eigenvalues are reliable. Many spurious eigenvalues can be generated. However, this method gives the projected density of states with good accuracy. If one is to analyze this algorithm, it can be seen that the Lanczos method is very efficient both in speed and in storage space. With the use of the recursion method, our problem is substantially simplified.

The choice of the initial state for the recursion method is determined by the optical matrix element between the valence bands and the conduction bands. For example, for the heavy-hole contributions, the initial state is given by

$$|0\rangle=\sum_{m,\mathbf{k}}\Psi^{e}_{n,\mathbf{k}}\Psi^{h0}_{m,3/2,-\mathbf{k}}O^{(3/2)}_{n,m} ,$$

where $\mathbf{k}$ under the summation runs over all mesh points selected. $O^{(\nu)}_{n,m}$, $\nu=\frac{3}{2},\frac{1}{2}$ are overlap integrals between the electron and hole envelope functions at $\mathbf{k}=0$, viz.,

$$O^{(\nu)}_{n,m}=\int f_{n,0}(z)g^{\nu}_{m,0}(z)dz .$$

In the actual computation, the Hamiltonian is defined in the electron-hole product states at the selected mesh points in $\mathbf{k}$ space. Thus the initial state is described by a column vector with components

$$G^{n}_{m,3/2}(\mathbf{k})=O^{(3/2)}_{n,m} \quad \text{for all } \mathbf{k} .$$

The excitonic states associated with different m, l, and ν will be coupled to the inital states via the exciton Hamiltonian as the iteration proceeds. In the calculation of the absorption coefficient, we multiply the density of states for the heavy-hole contributions by $CE_P/\hbar\omega$ and that for the light-hole contributions by $CE_P/3\hbar\omega$, where C is some constant, $\hbar\omega$ is the photon energy, and E_P is related to the momentum matrix element between the s-like conduction-band state and the x-like valence-band state at zone center by

$$E_P=2|\langle S|P_x|X\rangle|^2/m_0 .$$

Here m_0 is the free-electron mass. We have assumed a polarization vector parallel to the x direction (perpendicular to the growth direction). The factor 3 appearing in the denominator of the prefactor for the LHm-CBn transitions comes from symmetry considerations for the spin-orbit–coupled-valence-band Bloch states.

IV. RESULTS

A. Quantum wells

Figures 1 and 2 show the calculated absorption spectra (solid curves) of an 102-Å GaAs-$Al_{0.27}Ga_{0.73}As$ quantum well and an 81-Å GaAs-$Al_{0.26}Ga_{0.74}As$ quantum well, respectively. The Luttinger parameters used here are taken from Ref. 17 and the valence-band offset is taken to be 31% of the band-gap difference of GaAs and $Ga_{1-x}Al_xAs$.[18] The calculations include couplings of all s- and p-like excitonic (discrete plus continuum) states associated with the HH1-CB1, LH1-CB1, HH2-CB1, HH3-CB1, HH1-CB2, HH2-CB2, and LH1-CB2 transitions. 400 $k_{\|}$ points for each transition are used in the present calculations.

The corresponding photoluminescence excitation spec-

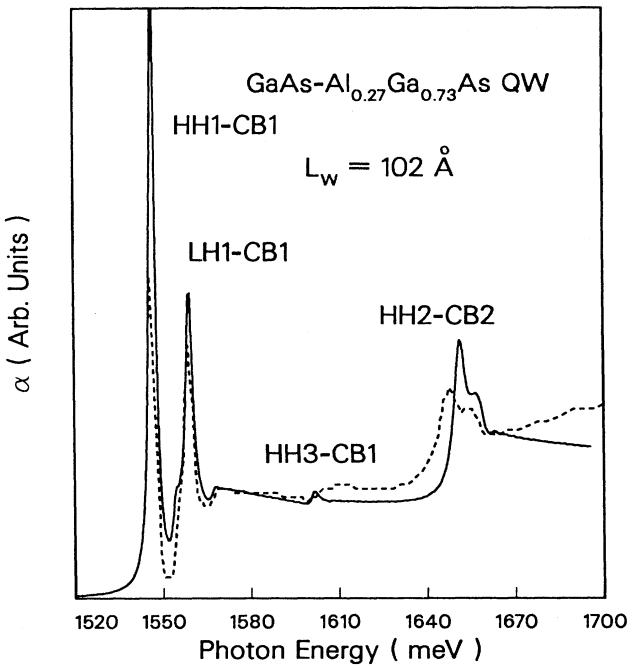

FIG. 1. Theoretical absorption spectrum (solid line) and experimental photoluminescence excitation spectrum taken from Ref. 4 (dashed line) for a 102-Å GaAs-$Al_{0.27}Ga_{0.73}As$ quantum well.

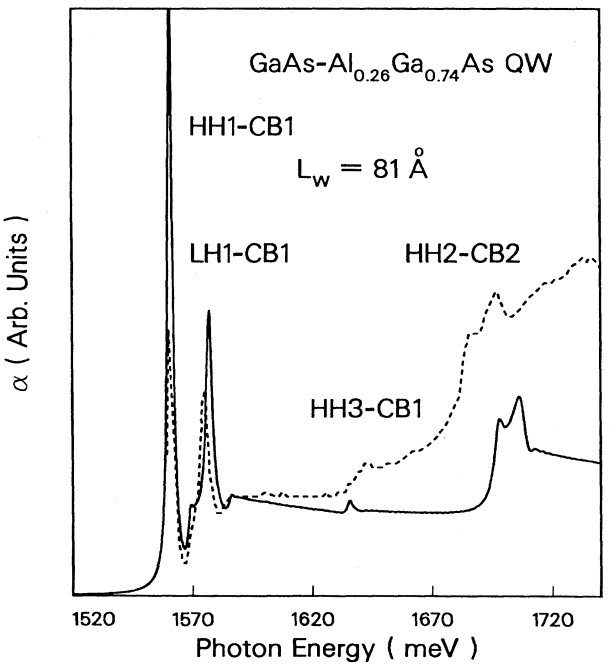

FIG. 2. Theoretical absorption spectra (solid line) and experimental photoluminescence excitation spectrum taken from Ref. 4 (dashed line) for an 81-Å GaAs-$Al_{0.26}Ga_{0.74}As$ quantum well.

tra obtained by Miller *et al.*[4] are reproduced (in dashed curves) for comparison. The most important feature of these spectra is the doublet structure labeled HH2-CB2. The splitting is a result of strong mixing of the 1*s* HH2-CB2 exciton with the 2*p* LH1-CB2 exciton. Without mixing the 2*p* LH1-CB2 exciton is forbidden. With mixing, the two exciton states share the oscillator strength of the HH2-CB2 transition. The overall absorption spectra predicted by our theory (with no adjustable parameters other than a uniform broadening of 1.2 meV for CB1 related transitions and 2.4 meV for CB2 related transitions) agree well with the experiment for both samples. In particular, the theory correctly predicts the variation of line shapes for the doublet structure associated with the HH2-CB2 transition when the well width changes from 102 Å to 81 Å. It should be noted that it is important to include the coupling of discrete exciton states (e.g., *p*-like LH1-CB2) with the continuum states of other excitons (e.g., *s*-like HH2-CB2). If one only includes the coupling of discrete excitonic states as was done in the variational calculations of Zhu,[6] the oscillator strength of the 2*p* LH1-CB2 exciton would be too small to account for the experimental data.

Another important feature in these figures is the small hump due to the HH3-CB1 exciton. This exciton is allowed even in the simple effective-mass model without valence-band mixing, because the overlap of HH3 and CB1 envelope functions is nonzero. The square of the overlap is equal to the ratio of oscillator strength of the HH3-CB1 exciton to that of the HH1-CB1 exciton in the effective-mass model. It can be shown that this overlap is sensitive to the valence-band offset. For example, the squared overlap integral for the 102-Å case is 0.000 18, 0.0062, and 0.011 for $Q_v = 0.15$, 0.31, and 0.4, respectively, where Q_v is the ratio of valence-band offset to the difference of GaAs and $Ga_{1-x}Al_xAs$ band gaps. The valence-band mixing effect is responsible for the predominant portion of the oscillator strength of the HH3-CB1 exciton.[2,3] The net effect is that the HH3-CB1 exciton has an oscillator strength of roughly 10% of the HH1-CB1 exciton oscillator strength, for values of Q_v between 0.15 and 0.4. Since the discrete HH3-CB1 exciton state is sitting in the continua of the HH1-CB1 and LH1-CB1 transitions, we expect to observe an interesting Fano-resonance effect.[19] Our theory described here is capable of predicting the realistic line shape of such Fano resonances. A close look of the Fano-resonance line shape due to the mixing of the HH3-CB1 exciton with the HH1-CB1 and LH1-CB1 continua is shown in Fig. 3. The dashed line in the figure represents the absorption coefficient without including the HH3-CB1 transitions. It is seen that the presence of the HH3-CB1 exciton gives rise to an asymmetric line shape, and it substantially modifies the spectrum due to continuum states, a result expected in Fano's theory. Unfortunately, it is difficult to compare this line shape with the experimental data, because it is sitting on a noisy background.

B. Superlattices

The absorption coefficients for excitonic states associated with the first conduction subband of a ($L_W = 75$ Å,

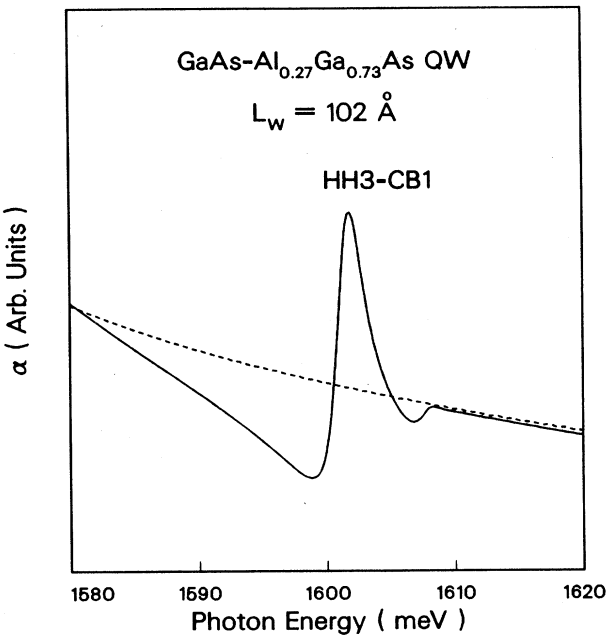

FIG. 3. Theoretical absorption spectra for a 102-Å GaAs-$Al_{0.27}Ga_{0.73}As$ quantum well near the HH3-CB1 transition with (solid curve) and without (dashed curve) the HH3-CB1 contribution.

$L_B = 105$ Å) GaAs-$Al_{0.18}Ga_{0.82}As$ superlattice and a ($L_W = 75$ Å, $L_B = 60$ Å) GaAs-$Al_{0.18}Ga_{0.82}As$ superlattice are shown in Fig. 4. The calculations include couplings of all *s*- and *p*-like excitonic (discrete plus continuum) states associated with the HH1-CB1, LH1-CB1, and HH2-CB1 transitions. We refer to this as a three-band model. In this figure, the dashed curve is due to the set of excitonic transitions involving predominantly HH1-CB1 *s*-like states, and the dotted curve is due to the set of excitonic transitions involving predominantly LH1-CB1 *s*-like states. The solid curve is the sum of the two. The vertical lines (dotted for HH1-CB1 and dashed for LH1-CB1) mark the onsets of continua and the positions of saddle points. To test the adequacy of the three-band model, we compare in Fig. 5 the valence-subband structures obtained by this model (dashed curves) and those obtained by solving the full $\mathbf{k}\cdot\mathbf{p}$ Hamiltonian (the "exact" model) (solid curves). The comparison shows that with only three zeroth-order valence-subband states included, the valence-subband structures are reasonably accurate for small wave vectors where the excitonic effect is most important. We have also repeated the calculation with the inclusion of two additional zeroth-order states (HH3 and HH4). We found that the valence-subband structures are improved substantially, but the difference in the absorption spectrum is negligible for the energy range of interest here.

High-resolution photoluminescence excitation (PLE) spectra for a large number of GaAs-$Al_xGa_{1-x}As$ superlattices including the two cases shown in Fig. 4 have recently been obtained by Song *et al.*[20] Comparing the absorption spectra for the two cases shown in Fig. 4, we see

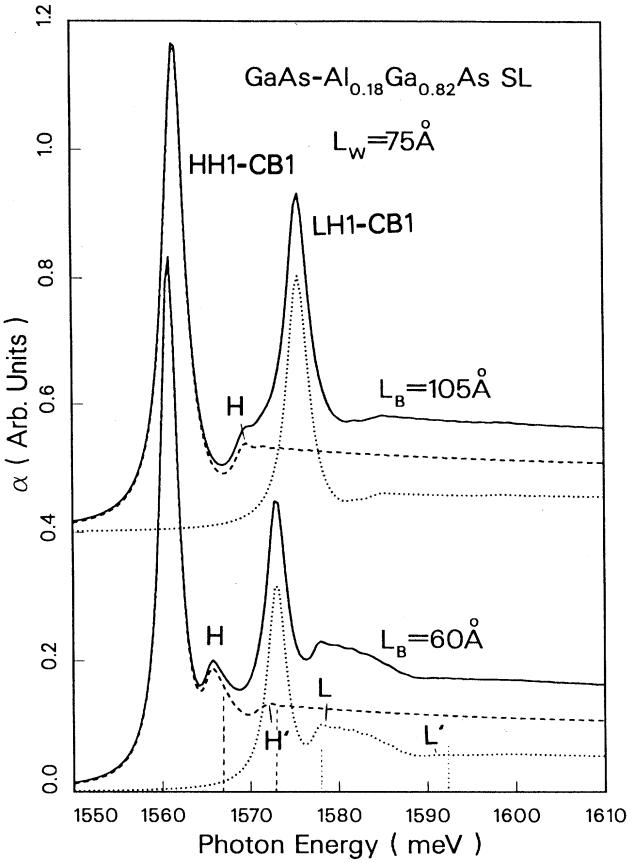

FIG. 4. Theoretical absorption spectra for GaAs-$Al_{0.18}Ga_{0.82}As$ superlattices with well width $L_W = 75$ Å and barrier widths $L_B = 105$ and 60 Å. Dashed line, HH1-CB1 contribution; dotted line, LH1-CB1 contribution; solid line, total.

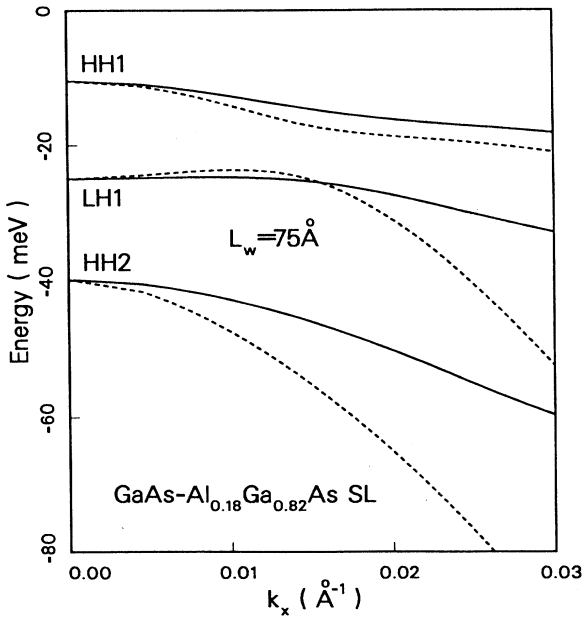

FIG. 5. Valence-subband structures of a ($L_W = 75$ Å, $L_B = 105$ Å) GaAs-$Al_{0.18}Ga_{0.82}As$ superlattice with $q = 0$. Solid line, exact model; dashed line, three-band model.

a clear difference in line shape as we change the well width from 105 Å to 60 Å. For the 105-Å case, the subband dispersion is negligible, and we have essentially uncoupled quantum wells. The shoulder structure just below the LH1-CB1 exciton (marked H) is associated with the $2s$ excited state of the HH1-CB1 exciton. For the 60-Å case, the subband dispersion is substantial (about 6 meV for HH1-CB1 and 14 meV for LH1-CB1), and we observe line-shape change due to the tunneling of excitons from one well to another. The most noticeable is the asymmetric line shape of the secondary peak structures marked H and L. These structures contain the closely spaced discrete exciton excited states (with predominant contribution from the $2s$) and the exciton resonances near the onsets of the continua. These features were observed by Song *et al.*,[20] and the line shapes obtained here are in good agreement with the experimental data. There are two other weak structures marked H' and L'. These structures are due to exciton resonances associated with the M_1 saddle points. The structure L' becomes more noticeable if we include more **k** points in our calculation. Evidence of the structure L' was observed by Song *et al.*[20] The structure H' is hidden under the LH1-CB1 exciton peak, so it was not resolved experimentally. In other samples examined by Song *et al.*[20] evidence for the structure H' was observed.

We have also calculated the absorption spectra of a series of GaAs-$Al_{0.23}Ga_{0.77}As$ superlattices with well width $L_W = 52$ Å and barrier width $L_B = 56$, 65, and 140 Å. The results are shown in Fig. 6. The dashed curves are due to excitonic transitions involving predominantly HH1-CB1 s-like states, and the dotted curves are due to excitonic transitions involving predominantly LH1-CB1 s-like states. The solid curve is the sum of the two. The vertical lines (dotted for HH1-CB1 and dashed for LH1-CB1) mark the onsets of continua and the positions of saddle points. Again, the main features other than the well-known principal exciton peaks include the $2s$ excited state followed by exciton resonances associated with the band minimum (marked by H and L) and the M_1 saddle-point exciton resonances (marked by H' and L'). The L' structures are not quite noticeable, but their presence is confirmed by magnifying the graph. The H' structure is observable for the $L_B = 65$ Å and 56 Å cases, since they are not hidden under the LH1-CB1 exciton, in contrast to the case shown in Fig. 4. Photoluminescence excitation (PLE) spectra of the series of samples have been measured by Deveaud *et al.*,[21] and the line shapes of the theoretical spectra presented here are also in excellent agreement with the experimental data. The structure H' associated with M_1 saddle-point exciton resonances was clearly identified for the $L_B = 65$ Å case.

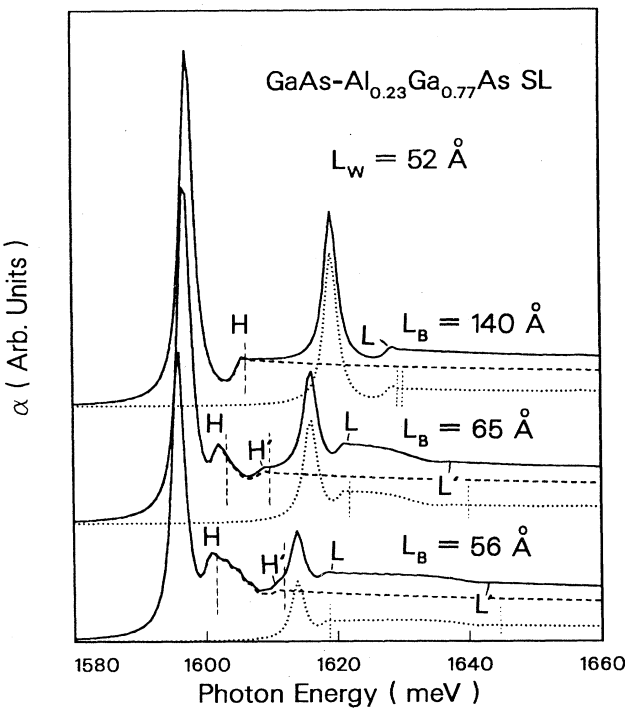

FIG. 6. Theoretical absorption spectra for GaAs-$Al_{0.23}Ga_{0.77}As$ superlattices with well width $L_W = 52$ Å and barrier widths $L_B = 140$, 65, and 56 Å. Dashed line, HH1-CB1 contribution; dotted line, LH1-CB1 contribution; solid line, total.

V. SUMMARY

In summary, we have incorporated the valence-band-mixing effect in our **k**-space sampling method to calculate the absorption spectra of realistic semiconductor quantum wells and superlattices. The band-mixing effect as well as the Fano-resonance effect give rise to interesting line shapes of the excitonic peaks in the absorption spectra. The line shapes predicted by our theoretical calculations are found in excellent agreement with those observed in the photoluminescence excitation (PLE) spectra.

ACKNOWLEDGMENTS

We would like to thank J. J. Song and B. Deveaud for fruitful discussions. This work was supported by the University of Illinois Materials Research Laboratory under National Science Foundation (NSF) Contract No. NSF-DMR-86-12860.

APPENDIX: COULOMB MATRIX ELEMENTS IN THE k-SPACE SAMPLING METHOD

In this Appendix, we provide derivations of the Coulomb potential matrix elements for the exciton basis states used in our **k**-space sampling method [see Eq. (2)].

For ideal 3D and 2D bulk systems, a basis state β_j contains the integration of electron-hole product states in a cube or square in $\mathbf{k}$-space centered at $\mathbf{k}_j$. Let $2a$ be the length of the sides for the cube or square. The matrix element between β_j and $\beta_{j'}$ is proportional to the integral

$$I=\int_{\mathbf{k}\in\Delta_j}d\mathbf{k}\int_{\mathbf{k}\in\Delta_j}d\mathbf{k}'\int d\mathbf{r}\,\frac{1}{r}e^{i\mathbf{k}\cdot\mathbf{r}-i\mathbf{k}'\cdot\mathbf{r}+i\,\Delta\mathbf{k}\cdot\mathbf{r}}\ ,$$

where $\Delta\mathbf{k}\equiv\mathbf{k}_j-\mathbf{k}_{j'}$. Integrating over $\mathbf{k}$ and $\mathbf{k}'$, we have

$$\begin{aligned}I&=4^d\int d\mathbf{r}\,\frac{1}{r}\prod_{i=1}^{d}\frac{\sin^2(ar_i)}{r_i^2}e^{i\,\Delta\mathbf{k}\cdot\mathbf{r}}\\&=4^d\frac{2}{\sqrt{\pi}}\int_0^\infty dt\int d\mathbf{r}\prod_{i=1}^{d}\frac{\sin^2(ar_i)}{r_i^2}e^{-t^2r^2+i\,\Delta\mathbf{k}\cdot\mathbf{r}}\\&=4^d a^{d+1}\frac{2}{\sqrt{\pi}}\int_0^\infty dt\prod_{i=1}^{d}F(t,\Delta k_i)\ ,\end{aligned}$$

where d is the dimensionality;

$$\begin{aligned}F(t,k)&=\int_{-\infty}^{\infty}dx\,e^{-t^2x^2+ikx}\sin^2x\\&=\tfrac{1}{2}\int_0^\infty du\int_{-\infty}^{\infty}dx\,e^{-(t^2+u)x^2+ikx}[1-\cos(2x)]\\&=\tfrac{1}{4}\int_0^\infty du\int_{-\infty}^{\infty}dx\,e^{-(t^2+u)x^2+ikx}(2-e^{2ix}-e^{-2ix})\\&=\tfrac{1}{4}\int_0^\infty du\left[\frac{\pi}{t^2-u}\right]^{1/2}\left[2\exp\left[-\frac{k^2}{4(t^2+u)}\right]-\exp\left[-\frac{(k+2)^2}{4(t^2+u)}\right]-\exp\left[-\frac{(k-2)^2}{4(t^2+u)}\right]\right]\\&=\frac{\sqrt{\pi}}{2}\int_0^{1/t}\frac{du}{u^2}(2e^{-w^2u^2}-e^{-(w+1)^2u^2}-e^{-(w-1)^2u^2})\ ,\end{aligned}$$

where $w\equiv k/2a$. Integrating by parts, we have

$$\begin{aligned}F(t,k)&=\sqrt{\pi}\int_0^{1/t}du[(w+1)^2e^{-(w+1)^2u^2}+(w-1)^2e^{-(w-1)^2u^2}-2w^2e^{-w^2u^2}]\\&\quad+\frac{\sqrt{\pi}t}{2}\left[\exp\left[-\frac{(w+1)^2}{t^2}\right]+\exp\left[-\frac{(w-1)^2}{t^2}\right]-2\exp\left[-\frac{w^2}{t^2}\right]\right]\\&=\frac{\pi}{2}G(t,w)\ ,\end{aligned}$$

where

$$\begin{aligned}G(t,w)&=|w+1|\,\mathrm{erf}\left[\frac{|w+1|}{t}\right]+|w-1|\,\mathrm{erf}\left[\frac{|w-1|}{t}\right]-2|w|\,\mathrm{erf}\left[\frac{|w|}{t}\right]\\&\quad+\frac{1}{\sqrt{\pi}}t(e^{-(w+1)^2/t^2}+e^{-(w-1)^2/t^2}-2e^{-w^2/t^2})\ .\end{aligned}\tag{A1}$$

Finally the matrix element between states β_j and $\beta_{j'}$ is

$$v(j,j')=\frac{I}{(4\pi a)^d}=\frac{2a}{2^d\sqrt{\pi}}\int_0^\infty dt\prod_{i=1}^{d}G(t,w_i)\ .\tag{A2}$$

It can be shown that the integral converges when $d>1$. The above formula can be also derived from the $\mathbf{k}$ space directly. Since the Fourier transforms of Coulomb function in $\mathbf{k}$ space with different dimensions are different, the derivation given above is more systematic. The derivations given above are for systems lacking spherical symmetry such as the tight-binding model crystal reported in Ref. 13.

For superlattices with a circular symmetry in the plane, we choose the exciton basis states of orbital angular momentum l to be the average of electron-hole product states over a ring, Δ_j in $\mathbf{k}$ space centered at $(k_\parallel^{(j)},q_j)$, viz.,

$$\beta_j^{nlm\nu}=\sum_{\mathbf{k}\in\Delta_j}e^{il\phi}\Psi^e_{n,\mathbf{k}}\Psi^{h0}_{m,\nu,-\mathbf{k}}/\sqrt{\Omega}\ ,$$

where $\Omega\equiv\sum_{\mathbf{k}\in\Delta_j}=\Delta/(2\pi)^3$ with Δ being the $\mathbf{k}$-space volume of the ring. The Coulomb matrix element between two exciton basis states $\beta_j^{nlm\nu}$ and $\beta_{j'}^{nlm'\nu}$ is approximately given by [see Eqs. (11) and (12)]

$$v^{nl}_{m,m',\nu}(j,j')\approx-\frac{4\pi e^2}{\epsilon}\sum_s F^e_n(q_j,q_{j'}-sK)F^h_{\nu,m,m'}(q_j,q_{j'}-sK)I_s^{(l)}(j,j')/(2\pi)^3\ ,\tag{A3}$$

where $K=\pi/d$, d is the length of the superlattice period, and

$$I_s^{(l)}(j,j')\equiv\frac{1}{\Delta}\int_{\mathbf{k}\in\Delta_j}d\mathbf{k}_\parallel\,dq\int_{\mathbf{k}\in\Delta_{j'}}d\mathbf{k}'_\parallel\,dq'\frac{e^{il(\phi-\phi')}}{|\mathbf{k}_\parallel-\mathbf{k}'_\parallel|^2+|q-q'+sK|^2}\ . \tag{A4}$$

In the above integral, $\mathbf{k}$ and $\mathbf{k}'$ are restricted in rings j and j', respectively. Here we have approximated the functions $F_n^{(e)}$ and $F^h_{\nu,m,m'}$ by their values at $q=q_j$ and $q'=q_{j'}$. This is a good approximation as long as the mesh size of q is small compared to K, since the two functions are quite smooth over the superlattice minizone. Below, we shall derive approximate expressions for the integrals $I_s^{(l)}(j,j')$ for $l=0$, and 1.

(i) $l=0$. We approximate the integral $I_s^{(0)}(j,j')$ by replacing the integrand by its value at $\mathbf{k}'_\parallel=\mathbf{k}_\parallel^{(j')}$ and $q'=q_{j'}$. Here $\mathbf{k}_\parallel^{(j')}$ can be any two-dimensional wave vector with length $k_\parallel^{(j')}$, because the integral is invariant under any rotation about the z axis. Thus we have

$$I_s^{(0)}(j,j')\approx\int_{\mathbf{k}\in\Delta_j}d\mathbf{k}_\parallel\,dq\frac{1}{|\mathbf{k}_\parallel-\mathbf{k}_\parallel^{(j')}|^2+|q-q_{j's}|^2}\ ,$$

where $q_{j's}\equiv q_{j'}-sK$. Here we have assumed that $k_\parallel\geq k'_\parallel$. With the change of variables, $\mathbf{k}_p\equiv\mathbf{k}_\parallel-\mathbf{k}_\parallel^{(j')}$, we obtain

$$\begin{aligned}I_s^{(0)}(j,j')&=\int_0^\pi d\phi_p\int_{q_j-\delta_1/2}^{q_j+\delta_1/2}dq\int_{k_{p-}}^{k_{p+}}dk_p^2\frac{1}{k_p^2+|q-q_{j's}|^2}\\&=\int_0^\pi d\phi_p\int_{q_j-\delta_1/2}^{q_j+\delta_1/2}dq\,\ln\left[\frac{k_{p+}^2+|q-q_{j's}|^2}{k_{p-}^2+|q-q_{j's}|^2}\right],\end{aligned} \tag{A5}$$

where

$$k_{p\pm}=[(k_\parallel^{(j)}\pm\delta_2/2)^2-k_\parallel^{(j')^2}\sin^2\phi_p]^{1/2}-k_\parallel^{(j')}\cos\phi_p\ ,$$

ϕ_p is the azimuthal angle for $\mathbf{k}_p$, δ_1 is the mesh size for q, δ_2 is the mesh size for $k_\parallel$. The integration over q can be carried out analytically. The final integration over ϕ_p is carried out numerically.

Alternatively, we can evaluate the integrals "exactly" by converting the integration over both $\mathbf{k},q$ and $\mathbf{k}',q'$ in Eq. (A4) to a one-dimensional integral. The resulting expressions are too complicated to be presented here. Furthermore, we found that the absorption spectra obtained by using the approximate integrals described above are almost identical to those obtained by using the exact integrals.

(ii) $l=1$. For the p-like states, we can write

$$I_s^{(1)}(j,j')=\frac{\pi}{\Delta}\int dk_\parallel\int dk'_\parallel\int dq\int dq'\int d(\phi-\phi')\frac{b\cos(\phi-\phi')}{c-b\cos(\phi-\phi')}\ , \tag{A6}$$

where $c\equiv k_\parallel^2+k_\parallel'^2+(q-q')^2$ and $b\equiv 2k_\parallel k'_\parallel$. Using the relation

$$\frac{b\cos(\phi-\phi')}{c-b\cos(\phi-\phi')}=\frac{c-b}{c-b\cos(\phi-\phi')}-1+\frac{b}{c-b\cos(\phi-\phi')}\ ,$$

we immediately obtain

$$I_s^{(1)}(j,j')=\frac{2\pi^2}{\Delta}\int dk_\parallel\int dk'_\parallel\int dq\int dq'\left[\left[\frac{c-b}{c+b}\right]^{1/2}-1\right]+I_s^{(0)}(j,j')\ . \tag{A7}$$

The first term on the right-hand side is a smooth function of variables $k_\parallel,k'_\parallel,q,q'$, so it can be approximated by the average value of the integrand or integrated numerically by Gaussian quadrature techniques.

[1]A. C. Gossard, P. M. Petroff, W. Wiegman, R. Dingle, and A. Savage, Appl. Phys. Lett. **29**, 323 (1976); E. E. Mendez, L. L. Chang, C. A. Chang, L. F. Alexander, and L. Esaki, Surf. Sci. **142**, 215 (1984).

[2]Y.-C. Chang and J. N. Schulman, Appl. Phys. Lett. **43**, 536 (1983); Phys. Rev. B **31**, 2069 (1985).

[3]G. D. Sanders, Y.-C. Chang, Phys. Rev. B **31**, 6892 (1985); **32**, 4282 (1985); **35**, 1300 (1987).

[4]R. C. Miller, A. C. Gosard, G. D. Sanders, Y.-C. Chang, and J. N. Schulman, Phys. Rev. B **32**, 8452 (1985).

[5]B. Zhu and K. Huang, Phys. Rev. B **36**, 8102 (1987).

[6]B. Zhu, Phys. Rev. B **37**, 4689 (1988).

[7]J. C. Phillips, in *Solid State Physics,* edited by S. Seitz, D. Turnbull, and H. Ehrenreich (Academic, New York, 1966), Vol. 18, p. 56; Phys. Rev. A **136**, 1705 (1964).

[8]B. Velicky and J. Sak, Phys. Status Solidi **16**, 147 (1966).

[9]H. Kamimura and K. Nakao, J. Phys. Soc. Jpn. **24**, 1313 (1968).

[10]E. O. Kane, Phys. Rev. **180**, 852 (1969).

[11]J. E. Rowe, F. H. Pollak, and M. Cardona, Phys. Rev. Lett. **22**, 933 (1969).

[12]S. Antoci, E. Reguzzoni, and G. Samoggia, Phys. Rev. Lett. **24**, 1304 (1970).

[13]H. Chu and Y.-C. Chang, Phys. Rev. B **36**, 2946 (1987).

[14]J. M. Luttinger and W. Kohn, Phys. Rev. **97**, 869 (1956).

[15]A. Fasolino and M. Altarelli, in *Two-Dimensional Systems, Heterostructures, and Superlattices,* edited by G. Bauer, F. Kucher, and H. Heinrich (Springer-Verlag, New York, 1984);

M. Altarelli, Phys. Rev. B **32**, 5138 (1985).
[16]G. Grosso and G. Pastori Parravicini, in *Memory Function Approaches to Stochastic Problems in Condensed Matter* [Adv. Chem. Phys. **62**, 81 (1985)]; D. M. Woodruff, S. M. Anlage, and D. L. Smith, Phys. Rev. B **36**, 1725 (1987).
[17]P. Lawaetz, Phys. Rev. B **4**, 3460 (1971).
[18]D. J. Wolford, T. F. Keuch, J. A. Bradley, M. A. Gell, D. Ninno, and M. Jaros, J. Vac. Sci. Technol. B **4**, 1043 (1986).
[19]U. Fano, Phys. Rev. **124**, 1866 (1961).
[20]J. J. Song, P. S. Jung, Y. S. Yoon, H. Chu, Y.-C. Chang, and C. W. Tu, Phys. Rev. B **39**, 5562 (1989).
[21]B. Deveaud, A. Chomette, F. Clerot, A. Regreny, J. C. Maan, R. Romestain, G. Bastard, H. Chu, and Y.-C. Chang, Phys. Rev. B (to be published).